WIND TUNNEL EXPERIMENTS AND CFD SIMULATIONS STUDY TO INVESTIGATE THE EFFECTS OF ROUGHNESS ON SHIP RESISTANCE

M.L. Hakim[1], N. Maqbulyani[1], B. Nugroho[2], I.K. Suastika[1], and I.K.A.P. Utama[1*]

[1] Department of Naval Architecture,
Institut Teknologi Sepuluh Nopember,
Surabaya, 60111, Indonesia

[2] Department of Mechanical Engineering,
The University of Melbourne,
Victoria, 3010, Australia

*Corresponding Author's Email: kutama@na.its.ac.id

ABSTRACT: A study on the influence of hull roughness on ship efficiency will be discussed in this report. The overall aim of this work is to show that directly comparing hull roughness from experiment and numerical work requires more than just one roughness characteristics, i.e average roughness height k_a. Other components such as solidity, slope, and compactness, would directly influence the flow. This work also further emphasises the importance of using sand grain equivalent roughness height k_s as a roughness reference. The increase of total drag coefficient (C_T) on a ship model due to $k_a$and k_s for both experiment and numerical investigation will be discussed.

Keyword: *Ship Resistance; Wind Tunnel Experiment; Computational Fluid Dynamics (CFD); Roughness; Biofouling.*

1.0 INTRODUCTION

In the last two decades, the issue of global warming, climate change, and the quality of emissions from operating ships has attracted plenty of attention from the International Maritime Organization (IMO). Approximately 95% of trade cargoes throughout the world are transported by ship [1], hence it has a large economic footprint. IMO notes that all maritime activities throughout the world produce total CO_2 as much as 2.2% compared to all CO_2 emissions due to all human activities [2], and it is predicted to increase by 50% - 250% in 2050 [3]. To address this issue, IMO issued new regulation via Energy Efficiency Design Index (EEDI) [4] and Ship Energy Efficiency Management Plan (SEEMP) program [5], in which ship designer and operator must adhere.

Although these measures have helped in lowering energy usage and emission, one effective method for saving energy on ships is through managing hull cleanliness from biofouling growth [6] [7]. Biofouling causes ship hull surface to become rough and lead to an increase in the friction resistance and energy requirements [8] [9] [10] [11]. Demirel et al [12] shows the increase of resistances (ΔC_F) up to 163.2% at 24 knots for KRISO Container Ship (KCS) due to calcareous fouling. According to Kodama et al [13], a large bulk carrier has a composition of friction resistance around 80-90%, thus the amount of energy loss due to biofouling is immense.

Due to its complexity, predicting ship drag penalty due to hull roughness is notoriously challenging because there are many different roughness components that can influence the increase in drags, such as size, compactness, height, etc [8,9]. Therefore, even after 50 years, there are still plenty of debates regarding a proper way to estimate ship drag penalty due to hull

roughness. An important step in assessing surface roughness is by obtaining the equivalent sand-grain roughness (k_s), skin friction velocity (U_τ) and roughness function (ΔU^+) [19-25], which can be obtained by imposing a rough walled surface/model onto a moving fluid. The issue with this method is the time and apparatus cost. One would need large wind tunnel or water tunnel to conduct such study. To bypass this, one would use Computational Fluid Dynamics (CFD) technique, such as Direct numerical Simulation (DNS), Large Eddy Simulation (LES), or RANS (Reynolds Averaged Numerical Simulation). Among all these three methods, RANS is the least expensive. However, it has limited accuracy, particularly in resolving the small-scale structures near the surface. Despite its limitation, RANS is widely used due to its application are mostly involves large-scale flow and it is considered sufficient for many engineering applications simulation.

In this study we will conduct both experiment and RANS CFD that looking into the influence of hull roughness on ship hydrodynamics. For the experiment, two ship hull models were tested, where one is smooth and another is rough. For the rough hull case, we use sandpaper to imitate fouled hull. Using the same hull model, RANS-based CFD simulations are also carried out.

2.0 MATERIALS AND METHODS

2.1 Separation of the Ship Resistance Components

The total ship resistance, R_T, can be divided into several resistance components, namely, the frictional resistance, R_F, and the residuary resistance, R_R, as given by Equation 1 [18].

$$R_T = R_F + R_R \tag{1}$$

Friction resistance occurs because the fluid layer that attaches to the hull wall, which has the same velocity as the ship, rubs against the fluid layer that is stationary and located away from the wall. Residual resistance is a phenomenon of pressure which consists of wave resistance R_W and viscous pressure R_{VP}, hence residuary resistance can be expanded R_R into equation 2.

$$R_T = R_F + R_{VP} + R_W \tag{2}$$

R_{VP} can be expanded further into kR_F as shown below.

$$R_T = R_F + kR_F + R_W = (1 + k)R_F + R_W \tag{3}$$

These resistance components are usually transformed in a non-dimensional form by dividing with dynamic pressure and wet surface area (WSA) as shown in Equation 4. This would lead to 5 and 6, where C_T is the total friction coefficient, C_F is the friction resistance coefficient, C_R is the residual resistance coefficient, C_{VP} is the viscous pressure coefficient, and C_W is the wave resistance coefficient, ρ is density of the used fluid, S is wet surface area (wsa) and U is the velocity. Note that C_W is also 0 due to the absence of wave.

$$C_T = \frac{R_T}{\frac{1}{2}\rho S U^2}; \qquad C_F = \frac{R_F}{\frac{1}{2}\rho S U^2}; \qquad C_{VP} = \frac{R_{VP}}{\frac{1}{2}\rho S U^2}; \quad C_W = \frac{R_W}{\frac{1}{2}\rho S U^2} \tag{4}$$

$$C_T = C_F + C_R \tag{5}$$

$$C_T = C_F + C_{VP} + C_W = (1 + k)C_F + C_W \tag{6}$$

2.2 Wind Tunnel Experiments

The cargo ship hull models that is tested for the wind tunnel experiment is scaled and the specific dimensions are described in Table 1. For the wind tunnel test, the hull was cut from the baseline to the line draught, hence only the WSA was used (see figure 1(left)). The wind tunnel has a test cross section L = 100 cm, B = 40 cm and H = 40 cm. Here the ship model is attached to a USCELL SP2-C3 load cell and it is placed in the middle of the tunnel.

Table 1: The particular dimensions of the models.

Items	Value	Unit	Items	Value	Unit
LoA	0.50	m	T	0.033	m
Lpp	0.47	m	Volume Displacement	1.0282×10^{-3}	m^3
Lwl	0.49	m	WSA	0.0565	m^2
B	0.084	m	C_B	0.743	

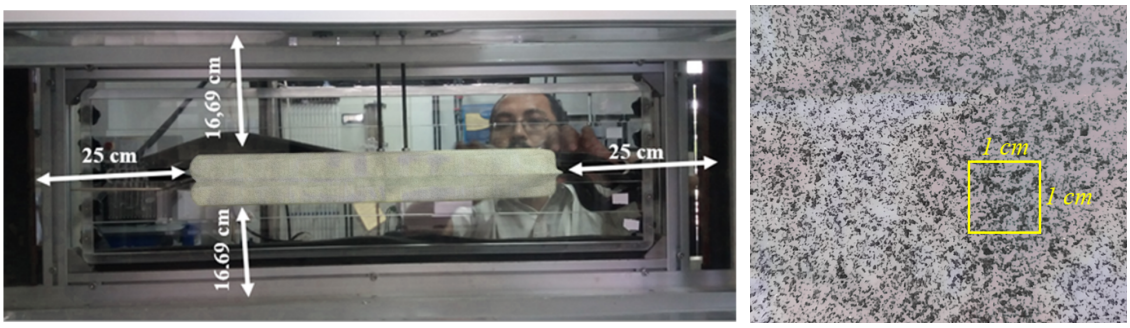

Figure 1: (Left) the rough model and its position in the test section, (Right) The physical roughness with average roughness height $k_a = 150$ µm.

In this experiment, we have prepared two different models: smooth walled hull and rough walled hull. For the rough model case, the roughness grains were obtained from burned sandpaper which then attached to the hull model. The sandpaper used has an average roughness height of $k_a = 150$ µm (see figure 1(right)). Here the smooth and the rough model were exposed to four different free stream velocities, namely 6, 10, 15 and 20 m/s. These in turn, lead to Reynolds number 1.98×10^5; 3.31×10^5; 4.96×10^5; and 6.61×10^5 respectively.

2.3 CFD Simulations

In this study, we use a commercial package FLUENT from ANSYS. Here the CFD simulations are carried out using the same hull model as the experiments.

2.3.1 Mathematical Formulation and Governing Equations

Here we use RANS (Reynold Averaged Navier-Stokes) based numerical solver where the governing equations consist of continuity (Equation 7) and incompressible Navier-Stokes (Equation 7). Here: U_i is the averaged velocity component; P is the mean pressure; f_i is the body force component of fluid; ρ is the fluid density; ν is the kinematic viscosity; u_i' is the fluctuation velocity component; $\overline{-\rho u_i' u_j'}$ is the Reynolds stress.

$$\frac{\partial U_i}{\partial x_i} = 0 \tag{7}$$

$$\frac{\partial U_i}{\partial t} + \frac{\partial (U_i U_j)}{\partial x_j} = -\frac{1}{\rho}\frac{\partial P}{\partial x_i} + \frac{\partial}{\partial x_j}\left[\nu\left(\frac{\partial U_i}{\partial x_j} + \frac{\partial U_j}{\partial x_i}\right)\right] - \frac{\partial \overline{u_i' u_j'}}{\partial x_j} + f_i \quad (8)$$

The turbulent model used in this calculation is SST k-ω which we found to be suitable for modelling both near wall flow and large scale flow further from the surface. The two equations consist of the equation of kinetic energy (Equation 9) and dissipation rate (Equation 10). Here P_k and P_ω denote the production terms of k and ω, respectively; β_k and β_ω are model constants, and C_ω represents the cross-diffusion term that appears in the transformed ω equation from the original ε equation. For SST k-ω, it is very important to take into account the distance of the wall or commonly called y^+. It is strongly recommended that the y^+ value is less than 2 especially for rough walled cases.

$$\frac{D(\rho K)}{D_t} = \nabla.\left[(\mu + \sigma_k \mu_I)\nabla K\right] + P_k + \beta_k \rho K \omega \quad (9)$$

$$\frac{D(\rho \omega)}{D_t} = \nabla.\left[(\mu + \sigma_\omega \mu_I)\nabla \omega\right] + P_\omega + \beta_\omega \rho \omega^2 + C_\omega \quad (10)$$

2.3.2 Hama Roughness Function ΔU^+ and Sand Grain Equivalent Roughness k_s

The drag force due to a rough surface can be calculated by classical log-law from the mean velocity profile in the turbulent boundary layer expressed in Equation 11. The mean velocity (U^+) is the flow velocity at each layer from the wall to outside the boundary layer. Then κ is the Von Karman constant, y^+ is the normal distance of U^+ to the wall, and B is the intercept log-wall for smooth surfaces. Hama roughness function ΔU^+ represents the increase in drag penalty, formulated in Equation 12, where there is a parameter k_s^+ (roughness Reynolds number). k_s^+ is expressed in Equation 13 where it represents the equivalent sand grain roughness height [19], U_τ is defined from $\sqrt{\tau_w/\rho}$, ν is kinematic viscosity. Note that although both k_a and k_s have the same unit height, k_s can only be obtained by imposing the roughness onto moving fluid.

$$U^+ = \frac{1}{\kappa} ln(y^+) + B - \Delta U^+ \quad (11)$$

$$\Delta U^+ = \frac{1}{\kappa} ln(k_s^+) + A - B \quad (12)$$

$$k_s^+ = \frac{k_s U_\tau}{\nu} \quad (13)$$

Schultz [9] classified the value of a ship's hull fouling condition in the range of k_s based on his experimental study as following: Hydraulically smooth surface = 0 ; Typical as applied Anti-fouling coating = 30 μm; Deteriorated coating or light slime = 100 μm; Heavy slime = 300 μm; Small calcareous fouling or weed = 1000 μm; Medium calcareous fouling = 3000 μm; Heavy calcareous fouling = 10000 μm.

For the CFD simulations we use commercial softrware Fluent, where there is a code for the wall-function approach as roughness function (ΔU^+) to fouling conditions with details on Equation 14. The equation is adopted from Cebeci and Bradshaw based on Nikuradse's data [16], where the value of C_s, in this study, was taken 0.26 based on Atencio et al [17]. The roughness function has a few differences when it is compared with what was done by Demirel et al [12] and Schultz & Flack [21], where the plots can be seen in Figure 2. In the current simulations, four variations of

velocities were carried out similar to the experiment. Thus the roughness variations consist of k_s = 0, 30, 300, 1000, and 3000 μm.

$$\Delta U^+ = \begin{cases} 0 \ \ for \ \ k_s^+ \leq 2.25 \\ \frac{1}{\kappa}\ln\left[\frac{k_s^+ - 2.25}{87.75} + C_s k_s^+\right] \times \sin[0.4258(\ln k_s^+ - 0.811)] \ \ for \ \ 2.25 < k_s^+ \leq 90 \\ \frac{1}{\kappa}\ln(1 + C_s k_s^+) \ \ for \ \ k_s^+ > 90 \end{cases} \quad (14)$$

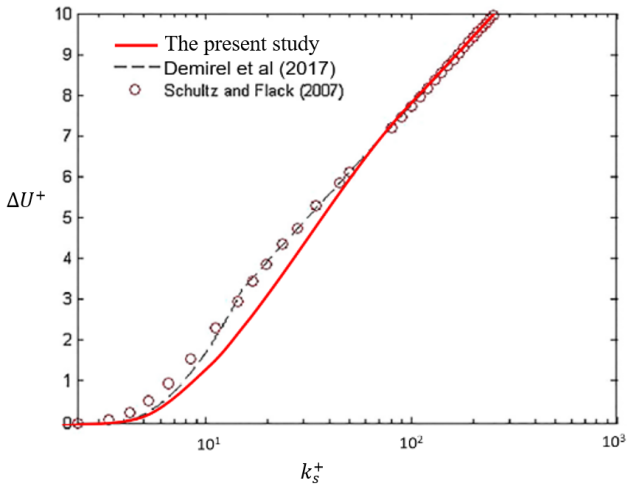

Figure 2: The proposed CFD roughness function model together with the roughness functions.

2.3.3 Boundary Conditions and Mesh Generation

The size of the computational domain was adjusted to represent the test section size of the wind tunnel. Because the domain has two symmetry axes, namely centre line and load line, the domain can be modelled for only a quarter of the full size to reduce the computational load. The upstream distance is set to have length 1 L, and the downstream is 3 L. Figure 3 shows the details of the domain size and boundary conditions, with set up as follows: A is velocity inlet; B is pressure outlet; C is vertical symmetry; D is horizontal symmetry; E and F (the test section wall) are no-slip and H (the hull model) are no-slip.

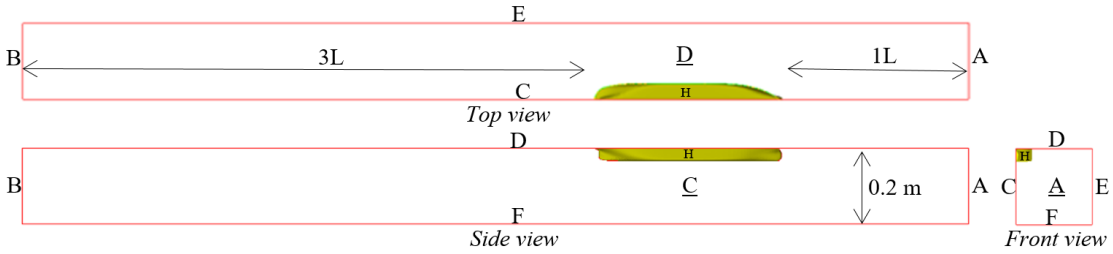

Figure 3: The domain size and the boundary conditions.

The boundary conditions are set based on the realistic flow conditions. Here the test section has a boundary surrounded by walls that have a friction effect, i.e no-slip condition. The inlet velocity boundary is set to have a turbulent intensity of 5%, and the viscosity ratio of 10 (based on the quality and the condition of the wind tunnel). The pressure outlet was set with 5% turbulent intensity and a viscosity ratio of 10 as well. The computational domain also requires settings for the fluid properties used and the solution method applied. The density of the air as input was 1,204

kg/m^3 and dynamic viscosity was 1.82×10^{-5} kg/ms, matching the condition of wind tunnels in an air-conditioned room. The descriptions of the solution method used were as follows: pressure-velocity coupling was simple; spatial discretization for the gradient was least-squares cell-based, for pressure was the second-order, for momentum, turbulent kinetic energy, and specific dissipation rate were the second order upwind. The residual of numerical calculation was set at 10^{-5} as the target to fulfil the convergence criteria. Figure 4 shows the 4 (four) million element array, which has a grid arrangement inflated on the model wall. The inflation is needed to get the y^+ value below 2 (two) because this simulation uses the SST k-ω turbulent model.

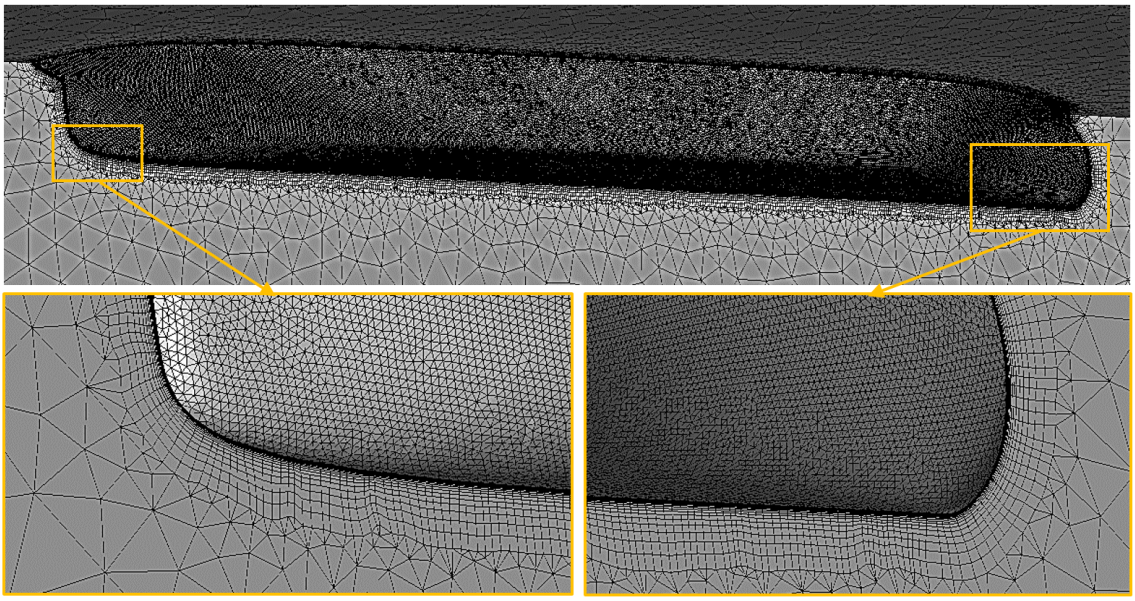

Figure 4: The appearance of mesh arrangement.

3.0 RESULT AND DISCUSSION

3.1 Experimental Results

Table 2: The experimental results

Re_L	Average $R_T \times 10^{-3}$ (N)				$C_T \times 10^{-3}$		ΔC_T (%)
	Smooth	Std. Dev	Rough	Std. Dev	Smooth	Rough	
1.98×10^5	12.8	2.14%	16.6	2.52%	10.372	12.904	24.41%
3.31×10^5	31.4	0.71%	43.3	1.32%	9.232	11.878	28.66%
4.96×10^5	68.0	1.87%	88.8	0.50%	8.938	12.518	40.06%
6.61×10^5	117.8	1.69%	149.2	1.55%	8.607	11.944	38.77%

The experimental results are summarized in Table 2, where the values are obtained from the measured force in the strain gauge as R_T and converted to RC_T with Equation 4. Each variation was tested repeatedly 5 times, and the results were counted the mean and the standard deviation, where the standard deviation is below 3%. Increasing the total resistance value (ΔC_T) from the velocity of 6 to 20 m/s on the model is 24 - 40%. The results of the experiment were compared with the numerical simulation results shown in Figure 5.

3.2 CFD Results

3.2.1 Grid Independence Study

Grid independence study is needed such that the numerical model can comply with the grit-independence criterion [22]. Table 3 described the grid independence study with 3 variations in the number and arrangement of the mesh. The results show that with around 4 million elements, the simulation can be valid and can be used for the other simulation variations. In this study, we use the medium mesh configuration to save computational time.

Table 3: The grid-independence result

Mesh configuration	Number of elements	R_T × 10^{-3} (N)	ΔR_T
Coarse	2,229,871	6.999	-
Medium	4,454,101	6.699	-4.49%
Fine	8,184,959	6.688	-0.16%

3.2.2 Verification study

To test the validity of our CFD simulation, we compare the numerical result with the friction coefficient (C_F) formula from ITTC 1957 [23]. Here we conducted simulation at four different velocities, namely 6 m/s, 10 m/s, 15 m/s and 20 m/s. Table 4 summarises the comparison between the experiment and numerical for the smooth wall case. The results show that there are less than 1% differences between the experiment and numerical, which we consider acceptable.

Table 4: The verification study results

Velocity (m/s)	Re×10^5	C_F ×10^{-3}		Δ%
		CFD	ITTC	
6	1.944	6.922	6.934	-0.18
10	3.241	6.084	6.085	-0.02
15	4.861	5.491	5.518	-0.49
20	6.481	5.130	5.162	-0.62

3.3 Total Resistance Results

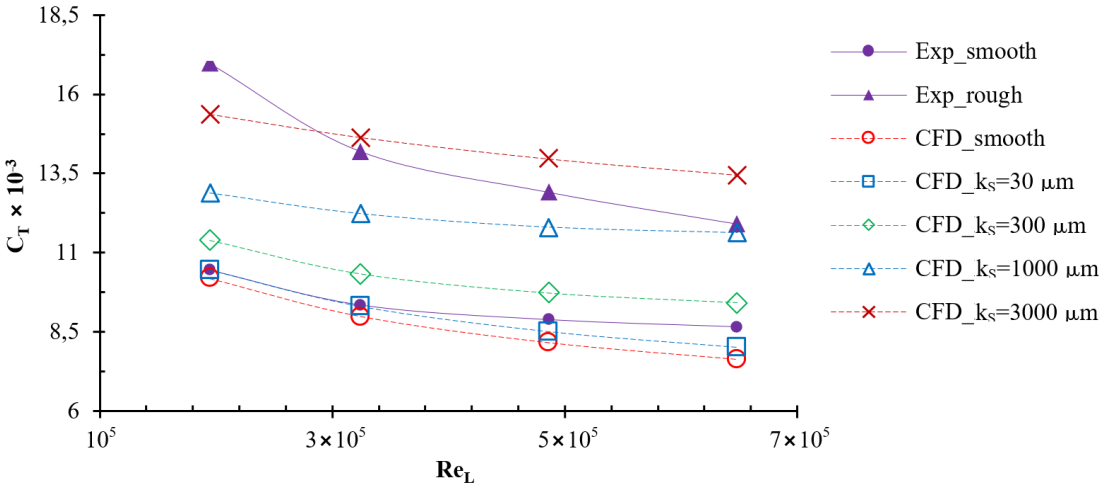

Figure 5: The comparison of the C_T result.

The total resistance (C_T) results from the CFD simulation are compared with the experimental results and plotted in Figure 5. The plot shows that the C_T value of the smooth model is very close to the CFD results of of k_s = 30 μm than that of the k_s = 0 μm, particularly at low Reynolds

number. The results may indicate that the smooth wall model is not hydrodynamically smooth. Unfortunately we do not have the necessary mean to scan the experimental model surface to check it's actual roughness height. Figure 5 also shows the comparison between the rough walled model and CFD. The data shows that the experimental results lie between k_s= 1000 µm and 3000 µm. A recent report from Squire et al [27] shows that a rough surface (sand paper) with k_a = 120 µm corresponds to k_s= 2000 µm. From observation, it seems that our experimental roughness lies around $k_s \approx$ 2500 µm. Note however that this is purely speculative, as we know that there are many factors that influence k_s values, such as solidity, average roughness height, effective slope, etc [23-27].

The change in sand grain equivalent roughness height clearly influences the coefficient of drag of an operating ship. As $k_s$increases, the ship's total resistance also increases significantly. Figure 6 shows the flow contour differences between a smooth walled surface and a highly rough surface k_s= 3000 µm. The main differences between the two profiles is the thickness of the boundary layer in the middle towards the stern part of the ship hull models. The rough walled surface experience a much thicker boundary layer than that of the smooth wall.

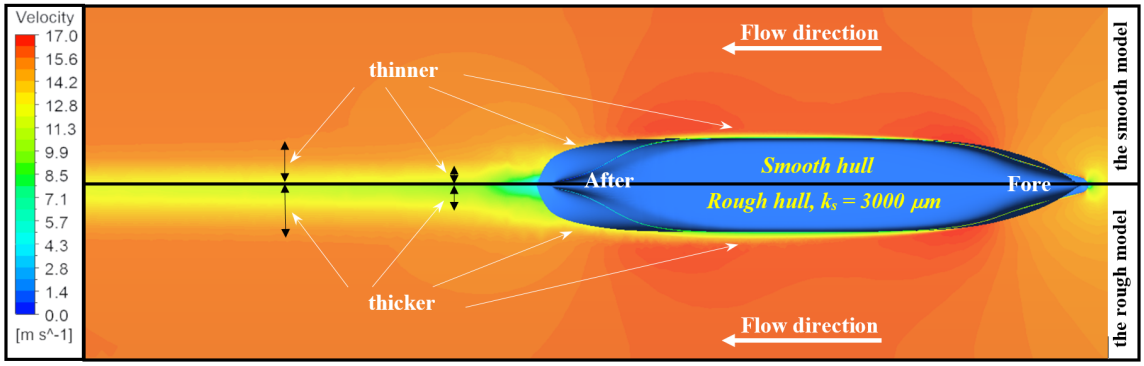

Figure 6: Velocity contour differences of smooth and rough models.

4.0 CONCLUSIONS

Wind tunnel experiments and CFD simulations have been carried out for investigating the increasing resistances due to roughness for a ship hull model. For the ship experiment we use grains from sand paper with average roughness height k_a = 150 µm as the roughness element. For the CFD cases, we tested four different sand grain equivalent roughness height k_s= 30, 300, 1000, and 3000 µm. The free stream velocities for both the experiment and numerical studies were set at 6, 10, 15, 20 m/s.

The results of C_T indicate that there are differences in the trend lines of relationship between Reynolds number and C_T for the experiments and the CFD simulations. The smooth walled experiment results however, is closer to the k_s = 30 µm of the CFD. This indicates that the smooth surface from the experiment is not hydrodynamically smooth. The rough experimental model with k_a = 150 µm has similarities with the CFD results between k_s = 1000 µm and more than 3000 µm. From observation, we believe that our experimental roughness lies around $k_s \approx$ 2500 µm. Note that this is purely approximation, because we do not have the surface scanning data of the experimental roughness and means to estimate the experiment's k_s value. For future studies, it is desirable to scan the ship hull model roughness directly via a laser or image surface scanner and replicate it onto the CFD model.

ACKNOWLEDGEMENT

The first author would like to thank the Ministry of Research, Technology and Higher Education Republic of Indonesia for funding his studies and research under the PMDSU batch 3 scheme at Institut Teknologi Sepuluh Nopember (ITS). This research was supported by the Energy Laboratory of Politeknik Elektronika Negeri Surabaya, the Hydrodynamics Laboratory of Department of Naval Architecture ITS, the Newton Fund Foundation and the British Council and the Australia Research Council.

REFERENCES

[1] RAEng, "Future Ship Powering Options," 2013.
[2] IMO, "Third IMO GHG Study 2014," 2015.
[3] IMO, "Second IMO GHG Study 2009," 2009.
[4] IMO. Annex 5, "Guidelines on the method of calculation of the attained Energy Efficiency Design Index (EEDI) for new ships," Resolution MEPC. 245(66), 2014.
[5] IMO. Annex 9, "Guidelines for the development of a Ship Energy Efficiency Management Plan (SEEMP)," Resolution MEPC.213(63), 2012.
[6] H. Wang, N. Lutsey, "Long-Term Potential for Increased Shipping Efficiency Through the Adoption of Industry-Leading Practices," International Council on Clean Transportation (ICCT), Washington, 2013.
[7] A. F. Molland, S. Turnock, D. Hudson, I. Utama, "Reducing Ship Emissions: A Review of Potential Practical Improvements in The Propulsive Efficiency of Future," *Transaction RINA: IJME*, vol. 156, no. A2, pp. 175-188, 2014.
[8] M.P. Schultz, "Effects of coating roughness and biofouling on ship resistance and powering," *Biofouling*, vol. 23, no. 5, pp. 331-341, 2007.
[9] I. Utama, B. Nugroho, "Biofouling, ship drag, and fuel consumption: A brief overview," *The Journal of Ocean Technology*, vol. 3, no. 2, pp. 43-48, 2018.
[10] M.L. Hakim, I. Utama, B. Nugroho, A.K. Yusim, M.S. Baithal, I K. Suastika, "Review of correlation between marine fouling and fuel consumption on ships," presented at SENTA 2017: 17th Conference on Marine Technology, Surabaya, Indonesia, 2017.
[11] M.L. Hakim, B. Nugroho, C. Chin, T. Putranto, I. Suastika, I. Utama., "Assessment of drag penalty resulting from the roughness of freshly cleaned and painted ship hull using Computational Fluid Dynamics," presented at 11th International Conference on Marine Technology (MARTEC), Kuala Lumpur, Malaysia, 2018.
[12] Y. K. Demirel, O. Turan, A. Incecik, "Predicting the effect of biofouling on ship resistance using CFD," *Applied Ocean Research*, vol. 62, pp. 100-118, 2017.
[13] Y. Kodama, A. Kakugawa, T. Takahashi, H. Kawashima, "Experimental study on microbubbles and their applicability to ships for skin friction reduction," *Int. J. Heat and Fluid Flow*, vol. 21, pp. 582-588, 2000.
[14] ITTC, "Specialist Committee on Surface Treatment-Final report and recommendations to the 26th ITTC," *Proceedings of 26th ITTC*, vol. II, 2011.
[15] S. Song, Y. K. Demirel, M. Atlar, "An investigation into the effect of biofouling on the ship hydrodynamic characteristics using CFD," *Ocean Engineering*, vol. 175, pp 122-137, 2019.
[16] T. Cebeci, P. Bradshaw, *Momentum Transfer in Boundary Layers*. New York: Hemisphere Publishing Corporation, 1977.
[17] B. N. Atencio, V. Chemoray, "A resolved RANS CFD approach for drag characterization of antifouling paints," *Ocean Engineering*, vol. 171, pp. 519-532, 2019.
[18] A. F. Molland, S. Turnock, D. Hudson, *Ship Resistance and Propulsion*. Cambridge: Cambridge university press, 2011.
[19] J. Nikuradse, "Laws of flow in rough pipe," *NACA Technical Memorandum*, 1292, 1933.

[20] L. Chan, M. MacDonald, D. Chung, N. Hutchins, A. Ooi, "A systematic investigation of roughness height and wavelength in turbulent pipe flow in the transitionally rough regime," *J. Fluid Mechanics*, vol. 771, pp. 743-777, 2015.

[21] M. P. Schultz, K. Flack, "The rough-wall turbulent boundary layer from the hydraulically smooth to the fully rough regime," *J. Fluid Mechanics*, vol. 580, pp. 381-405, 2007.

[22] J. Anderson, 1995, *Computational Fluid Dynamics: The Basics with Applications*. New York: McGraw-Hill Inc, 1995

[23] ITTC, "Performance Prediction Method," Procedure Number 7.5-02-03-01.4, 2002.

[24] Y. K. Demirel, M. Khorasanchi, O. Turan, A. Incecik, M. P. Schultz, "A CFD model for the frictional resistance prediction of antifouling coatings," *Ocean Engineering*, vol. 89, pp. 21-31, 2014.

[25] J. P. Monty, E. Dogan, R. Hanson, A. J. Scardino, B. Ganapathisubramani, N. Hutchins, "An assessment of the ship drag penalty arising from light calcareous tubeworm fouling," *Biofouling*, vol. 32, no. 4, pp. 451-464, 2016.

[26] I. Utama, B. Nugroho, C. Chin, M. L. Hakim, F. A. Prasetyo, M. Yusuf, I. Suastika, J. Monty, N. Hutchins, B. Ganapathisubramani, "A Study of Skin Friction-Drag from Realistic Roughness of a Freshly Cleaned and Painted Ship Hull," presented at International Symposium on Marine Engineering (ISME), Marine Engineering Society of Japan (MESJ, currently JIME), Tokyo, Japan, 2017.

[27] Squire, D.T., Morrill-Winter, C., Hutchins N., Schultz, M.P., Klewicki, J.C. & Marusic I. (2016) Comparison of turbulent boundary layers over smooth and rough surfaces up to high Reynolds numbers. ***J. Fluid Mech.*** **795**, 210-240